Cellular Dewetting: Opening of Macroapertures in Endothelial Cells

David Gonzalez-Rodriguez,[1,*] Madhavi P. Maddugoda,[2] Caroline Stefani,[2] Sebastien Janel,[3] Frank Lafont,[3]
Damien Cuvelier,[1] Emmanuel Lemichez,[2] and Françoise Brochard-Wyart[1]

[1]*Institut Curie, CNRS UMR 168 and Université Paris 6, 11 rue Pierre et Marie Curie, 75248 Paris Cedex 05, France*
[2]*INSERM, U1065, Université de Nice-Sophia-Antipolis, Centre Méditerranéen de Médecine Moléculaire, C3M,
Nice, F-06204 Cedex 3, France*
[3]*Center for Infection and Immunity of Lille, CNRS UM8204, INSERM U1019, Institut Pasteur de Lille,
Université Lille Nord de France, Lille-F59021, France*

Pathogenic bacteria can cross from blood vessels to host tissues by opening transendothelial cell macroapertures (TEMs). To induce TEM opening, bacteria intoxicate endothelial cells with proteins that disrupt the contractile cytoskeletal network. Cell membrane tension is no longer resisted by contractile fibers, leading to the opening of TEMs. Here we model the opening of TEMs as a new form of dewetting. While liquid dewetting is irreversible, we show that cellular dewetting is transient. Our model predicts the minimum radius for hole nucleation, the maximum TEM size, and the dynamics of TEM opening, in good agreement with experimental data. The physical model is then coupled with biological experimental data to reveal that the protein missing in metastasis (MIM) controls the line tension at the rim of the TEM and opposes its opening.

The endothelium is the inner cellular lining that separates blood vessels from the surrounding tissues. Pathogenic bacteria can induce the dysfunction and rupture of the endothelial barrier to colonize tissues, leading to major pathologies [1]. One way for pathogenic bacteria to cross the endothelial barrier is the opening of transcellular tunnels through the cell cytoplasm, termed transendothelial cell macroapertures (TEMs) [2,3]. Indeed, recent biological studies have unveiled the ability of several bacterial toxins, such as epidermal cell differentiation inhibitor (EDIN) of the bacterium *Staphylococcus aureus*, to trigger TEM opening in endothelial cells [3,4]. Upon penetration into the host cells, EDIN disrupts the formation of contractile actomyosin cable components of the cell cytoskeleton [5,6]. More precisely, EDIN ADPribosylates the small GTPase RhoA, which is a master regulator of actomyosin contraction through its capacity to stimulate Rho kinase and induce downstream phosphorylation of myosin light chain to promote actomyosin contractility [7]. This disruption of the contractile cytoskeleton network makes the cells spread [4,8] (Fig. 1). Cell membrane tension, no longer resisted by contractile fibers, induces the spontaneous opening of TEMs, which are transcellular holes through the cell cytoplasm around which the cell membrane adopts a toroidal shape (Fig. 1). While no direct evidence of TEM formation in live animals has yet been gathered, TEMs have been shown to form in the endothelium of rat arteries intoxicated or infected *ex vivo* [3,4].

Maddugoda *et al.* have recently characterized the biological mechanisms by which cells close TEMs [3]. Indeed, a striking characteristic of TEMs is that they are transient: they open up to a maximum size and they eventually close back. Maddugoda *et al.* identified the role of the protein missing in metastasis (MIM) in restricting TEMs. MIM accumulates at the curved membrane of the TEM edge in a few hundred milliseconds following opening [3]. Maddugoda *et al.* showed that a reduction of the cellular expression of MIM protein compromises the ability of cells to close TEMs [3]. However, the mechanism by which MIM controls TEM size remains unknown. In this article we present quantitative measurements of the dynamics of TEM opening and of the influence of MIM expression on TEM size. The new measurements reported
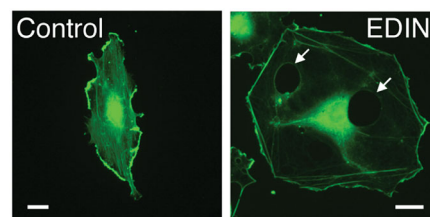

FIG. 1 (color). Immunofluorescence visualization of the actin cytoskeleton of human umbilical vein endothelial cells (HUVECs) under control conditions (i.e., before EDIN intoxication) and after being intoxicated with EDIN for 24 h, when several TEMs (indicated by arrows) are visible. Cells were fixed as described by Boyer *et al.* [4], and the actin cytoskeleton was labeled using TRITC-conjugated phalloidin (Sigma), which corresponds to the green signal in the images. The images show EDIN-induced cytoskeletal disruption and associated cell spreading, although residual actin pools remain present at the cell edges. The visualization was performed with a LSM510-Meta confocal microscope (Carl Zeiss) at 40 × magnification. The scale bars represent 10 μm.

here have been performed using the same experimental conditions described by Maddugoda *et al.* [3]. The reader is referred to this publication for full details on the experimental setup. Here we model the observations by an analogy with liquid dewetting, thus describing this biological phenomenon as a case of cellular dewetting.

A typical TEM opening event is shown in Figs. 2(a)–2(d) (see also movie 1 in the Supplemental Material [9]). Figures 2(a)–2(c) show a TEM opening in a human umbilical vein endothelial cell (HUVEC) cultured and intoxicated with recombinant purified EDIN toxin at 100 μg/ml for 24 h as described by Boyer *et al.* [4]. Note that the same phenomenon is shown at the scale of the whole cell in Fig. 1, right panel. TEMs start forming at about 3 h after intoxication, and the measurements presented here correspond to 24 h after intoxication. During intoxication and visualization, cells were placed on a gelatin-coated glass slide within a controlled environment chamber (5% CO_2, 37 °C) and recorded by phase contrast videomicroscopy using a Leica DMI6000 *B* inverted microscope at 20× magnification. Figure 2(d) shows the evolution of the TEM radius *R* as a function of the elapsed time. The opening is very fast for the first few seconds, then slows down, and at about 1 min the TEM appears stable at *R* around 5–10 μm. In a longer time scale the TEM closes back, eventually disappearing completely after about 10 min. This closing back is an active cellular process driven by actin-rich membrane waves emitted from the TEM edges [3], indicated by arrows in Fig. 2(c). In contrast, TEM opening and stabilization is a passive process that can be described by simple physical laws, as discussed in the following. Figure 2(e) shows the measured height

profile of a TEM in a HUVEC intoxicated with EDIN for 24 h. Profiles were obtained by atomic force microscopy (AFM) operated in contact mode using an ultrasoft Olympus Bio-Lever with a spring constant of 6 mN/m. A constant force of 100 pN was applied while scanning at 0.3 to 1 HZ. Experiments were performed at room temperature on a commercial stand-alone AFM (Bioscope II, Veeco Instrument) combined with an inverted optical microscope (Axiovert 200M, Zeiss). Profiles were extracted using Veeco's Nanoscope software. It is noted that AFM line scanning is fast compared to TEM opening. The measured profiles show the existence of a circular rim surrounding the TEM of a width *l* comparable to the TEM radius *R*. The height of the rim above the unaffected cell is comparable to the cell thickness $h \approx 50$ nm.

We interpret the TEM opening dynamics and its equilibrium maximum size through an analogy with liquid dewetting. Dewetting refers to the spontaneous withdrawal of a liquid film from a surface, by nucleation and growth of dry patches. The free energy *F* of a hole of radius *R* in a liquid film is the sum of two terms:

$$F = S\pi R^2 + 2\pi R \mathcal{T}. \tag{1}$$

The first term on the right-hand side of Eq. (1) is the gain of surface energy by drying the surface, where $S = W_{\text{dry}} - W_{\text{wet}} < 0$ is the spreading parameter, or the difference between the dry and wet surface energies per unit area. The second term is the line energy, which depends on the line tension $\mathcal{T}$. For constant *S*, *F* has a maximum for a critical radius $R_{\text{crit}} = \mathcal{T}/|\mathcal{S}|$. A hole of radius $R < R_{\text{crit}}$ spontaneously closes, while a hole of radius $R > R_{\text{crit}}$ spontaneously grows, being surrounded by a liquid rim that stores the liquid collected from the dry patch inside the hole. In the latter scenario, the advancement of the rim is driven by a force per unit length $|S|$ and opposed by a friction force. This dewetting process has been studied for a wide variety of liquids from water to ultraviscous pastes [10]. For a thin film of viscous liquid of dynamic viscosity ν deposited on a nonwetting solid substrate, the hole opens at a constant velocity of dewetting V_d [11]. The liquid collects in a rim surrounding the hole. The equation of motion of the rim results from a balance between the capillary driving force per unit length, $|S|$, and the friction force associated to the viscous dissipation in the two liquid wedges that bound the rim. Both forces are constant, leading to the hole opening at a constant velocity $V_d \sim (\gamma/\eta)\theta_E^3$, where θ_E is the equilibrium contact angle of a liquid drop deposited on the substrate. By contrast, ultraviscous liquids slide over the substrate when dewetting [12]. This sliding is characterized by an extrapolation length, *b*. If the film thickness *h* is much larger than the extrapolation length, $h \gg b$, the film flows like an ordinary viscous liquid discussed above. If the film thickness is smaller than the extrapolation length, $h < b$, the fluid flows at unison (plug flow) and the dominant dissipation occurs
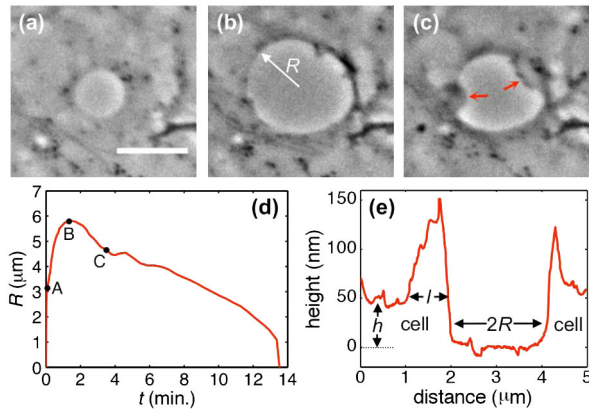

FIG. 2 (color online). (a)–(c) Sequence of a TEM opening event in a HUVEC intoxicated with EDIN for 24 h at (a) $t = 5$ s, (b) $t = 160$ s, and (c) $t = 210$ s after the opening starts. The scale bar represents 10 μm. (d) Time evolution of the TEM radius $R(t)$. The points *A*, *B*, and *C* correspond to the images (a), (b), and (c). It is noted that this particular event exhibits a closure time longer than usual (5–10 min). (e) Instantaneous vertical cross-sectional profile of a TEM obtained by atomic force microscopy.

at the solid-liquid interface. The balance of viscous and driving force per unit length of the contour yields

$$klV_d = |S|, \tag{2}$$

where $k \sim \eta/a$ is the coefficient of friction, the ratio of a viscosity devided by a molecular size, and $l \sim \sqrt{Rh}$, is the size of the rim, related by conservation of mass to the film thickness h and the radius of the hole R. Equation (2) yields a growth law of the hole $R(t) \sim [(|S|at)/(\eta h^{1/2})]^{2/3}$.

An analogous phenomenon to liquid film dewetting is the opening of pores in membranes. While liquid dewetting is driven by the spreading parameter, which is constant and leads to complete dewetting, pore opening is driven by the membrane tension, which decreases as the hole expands [13]. Thus, pores open up to a maximum size, which corresponds to the equilibrium of membrane and line tension.

Similar to pore opening in membranes, the driving force per unit length of contour for TEM opening is given by

$$F_d = 2\sigma - \frac{\mathcal{T}}{R}, \tag{3}$$

where σ is the cell plasma membrane tension, and $\mathcal{T}$ is the line tension, which is assumed constant. If the membrane tension is supposed constant and equal to the undisturbed membrane tension, $\sigma = \sigma_0$, a TEM will open if its radius R is larger than a critical nucleation radius, $R_n = \mathcal{T}/(2\sigma_0)$. If $R < R_n$, $F_d < 0$ and the hole will spontaneously close, while if $R > R_n$, $F_d > 0$ and the hole will grow. For liquid membranes, however, σ does not remain constant once the hole has formed, but it depends on the hole radius. As the hole increases, the excess membrane area increases, and σ decreases, as established by Helfrich's law [14]:

$$\frac{\sigma}{\sigma_0} = \exp\left\{-\frac{8\pi\kappa}{k_B T}\frac{R^2}{R_t^2}\right\} \equiv \exp\left\{-\frac{R^2}{R_c^2}\right\}, \tag{4}$$

where $\kappa \sim 40k_B T$ is the membrane bending rigidity [15], with k_B being the Boltzmann constant and T the temperature, R_t^2 is the area covered by the spread cell, and $R_c \equiv \alpha^{-1/2}R_t$, with $\alpha \equiv (8\pi\kappa)/(k_B T)$. Equations (3) and (4) lead to $F_d = 0$ for two values of the radius, corresponding to the two roots of the equation $2R\sigma = \mathcal{T}$. By defining the nondimensional variables $\tilde{R} \equiv R/R_c$ and $\tilde{\mathcal{T}} \equiv \mathcal{T}/(2\sigma_0 R_c)$, this equation can be written as

$$\tilde{R}\exp\{-\tilde{R}^2\} = \tilde{\mathcal{T}}. \tag{5}$$

A graphical representation of Eq. (5) is shown in Fig. 3(b), where the black curve corresponds to the nondimensional driving force [the left-hand side in Eq. (5)] and the four different horizontal lines illustrate four different values of the nondimensional resisting force (the line tension $\mathcal{T}$). TEM growth occurs for $R > R_n$ and stops at $R = R_m$. For very small $\tilde{\mathcal{T}}$, the solutions of Eq. (5) are approximately

given by $R_n \sim \mathcal{T}/(2\sigma_0)$ and $R_m \sim R_c(-\ln\tilde{\mathcal{T}})^{1/2}$. As $\mathcal{T}$ increases, the values of R_n and R_m get closer, both becoming equal to $R_c/\sqrt{2}$ for $\tilde{\mathcal{T}} = 1/\sqrt{2e} \approx 0.43$. Beyond this value of the line tension, Eq. (5) has no real solutions and no TEM can form. Approximate values of the parameters for the TEM observations discussed here are $h \approx 50$ nm, $\alpha \approx 1000$, and $R_t = 50$ μm. The membrane tension is of the order of $\sigma_0 \approx 10^{-5}$ N/m [16,17]. Since the line tension arises from the energetic cost to bend the membrane at the TEM edge, it can be estimated as $\mathcal{T} \approx 2\kappa/h \approx 5 \times 10^{-12}$ N [13]. These values result in a minimal nucleation radius of about $R_n \approx 0.1$ μm, which is below the observable diffraction limit, and a maximum TEM radius of $R_m \approx 5$ μm, consistent with the experimental observations [Figs. 2(d) and 3(a)].

We apply this model to interpret the role of MIM in controlling TEM maximum size. We have performed experiments to measure the maximum radius R_m of TEMs as a function of the MIM expression levels in EDIN-intoxicated cells, shown in Fig. 3(a). The figure presents the statistical distribution of R_m measured in four different conditions. Control intoxicated HUVECs exhibit typical
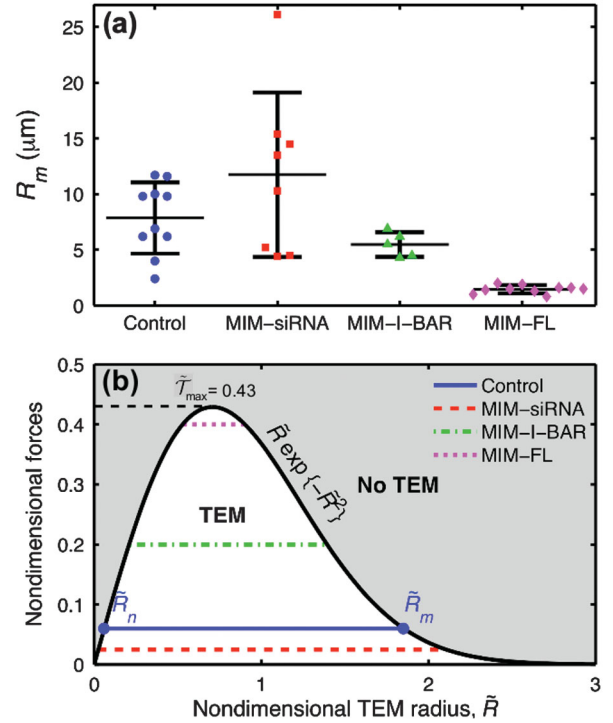

FIG. 3 (color). (a) Statistical distribution of TEM radii R_m observed for control HUVECs and for conditions of MIM knockdown (MIM-siRNA) and overexpression (MIM-I-BAR and MIM-FL). (b) Nondimensional driving and resisting forces ($\tilde{R}\exp\{-\tilde{R}^2\}$ and $\tilde{\mathcal{T}}$) as a function of the nondimensional TEM radius $\tilde{R}$. The intersection of the curve with a horizontal line represents the solutions of Eq. (5). The different horizontal lines illustrate different values of $\tilde{\mathcal{T}}$ and are plotted to interpret the experimental observations in (a).

R_m of about 5–10 μm. Next we studied MIM knockdown cells (labeled MIM-siRNA in Fig. 3), obtained by magnetofection technology (OZ Biosciences) with the siRNA- SMARTpool sc-77651 (Santa Cruz Biotech). MIM knockdown cells, which have up to a 75% loss of MIM expression compared to control, display a greater heterogeneity of TEM sizes and some very large TEMs not seen in control cells (e.g., R_m of 26 and 15 μm). In contrast, cell overexpression of the MIM I-BAR protein domain or of the full-length MIM protein (labeled MIM-I-BAR and MIM-FL in Fig. 3, respectively) result in dramatic reductions of R_m. Plasmid transfection was carried out by electroporation as previously described [4]. In parallel, our cellular dewetting model [Fig. 3(b)] predicts R_m to decrease as $\mathcal{T}$ is increased [i.e., as we move up through the different horizontal lines in Fig. 3(b)]. Combining the experiments and the model, we propose that MIM controls R_m and limits TEM opening by creating a line tension around the TEM by the scaffolding of MIM molecules along the edge. This is consistent with the fact that MIM senses membrane curvature and is recruited along the TEM edge [3]. This is a TEM-stabilizing mechanism independent of actin polymerization, which acts at longer time scales (several minutes) and plays a key role in TEM closing [3].

The dewetting model also describes the dynamics of TEM opening, which are governed by the balance between membrane tension, line tension, and friction. Since RhoA is known to control focal adhesion driven adhesion [18], we assume that the loss of RhoA activity upon EDIN intoxication will lead to decreased adhesion and that the cell slips on the substrate. Frictional dissipation is thus dominated by friction in the interface between the cell rim (of width l) and the substrate. This case is analogous to the dewetting of ultraviscous liquids described by Eq. (2). The balance between friction and driving force is

$$kl\dot{R} = 2\sigma(R) - \frac{\mathcal{T}}{R}, \qquad (6)$$

with $\sigma(R)$ given by Eq. (4) and $\mathcal{T}$ assumed constant. The radial extension l of the cell rim is related by mass conservation to h and R [see cross-sectional profile in Fig. 2(e)]. In ultraviscous dewetting, the cross-sectional area of the liquid rim scales as l^2. For TEM opening, however, the height of the rim remains constant and of the order of the cell thickness h, as discussed above [see Fig. 2(e)]. Consequently, mass conservation yields $l \sim R$. In nondimensional form, Eq. (6) yields

$$\int_{\tilde{R}_n}^{\tilde{R}} \frac{r^2}{r\exp\{-r^2\} - \tilde{\mathcal{T}}}\, dr = \tilde{t}, \qquad (7)$$

where $\tilde{t} = t/\tau$ is the nondimensional time, with $\tau \equiv kR_c^2/(2\sigma_0)$. The cell friction coefficient k has been experimentally estimated to be $k \approx 10^8$ Pa $\cdot$ s/m for cells slipping in a nonadhesive passive capillary tube [19], and $k \approx 10^9$ Pa $\cdot$ s/m for cells spreading on an adhesive substrate [20]. For $k = 10^8$ Pa $\cdot$ s/m, the characteristic time of opening is of the order of $\tau \approx 5$ s.

Figure 4(a) shows the experimentally measured dynamics of TEM opening for control HUVECs, as well as a numerical solution of Eq. (7) (dashed line) for the typical parameter values discussed above ($\tilde{\mathcal{T}} = 10^{-1}$, $\tau = 5$ s, $R_c = 3$ μm). The experimental measurements show a variability that leads to variable final TEM radii in the range of 2–12 μm. This spread is attributed to a variability in the line tension. Indeed, if we normalize the experimental measurements by their maximum radii [Fig. 4(b)], the experimental curves collapse and are well represented by the normalized theoretical prediction (full line). We note that, since $\tilde{\mathcal{T}} \ll 1$, the growth law at short time approximately scales as $\tilde{R} \sim \tilde{t}^{1/2}$. The TEM surface increases linearly with time, then the growth slows down to reach the maximum radius.
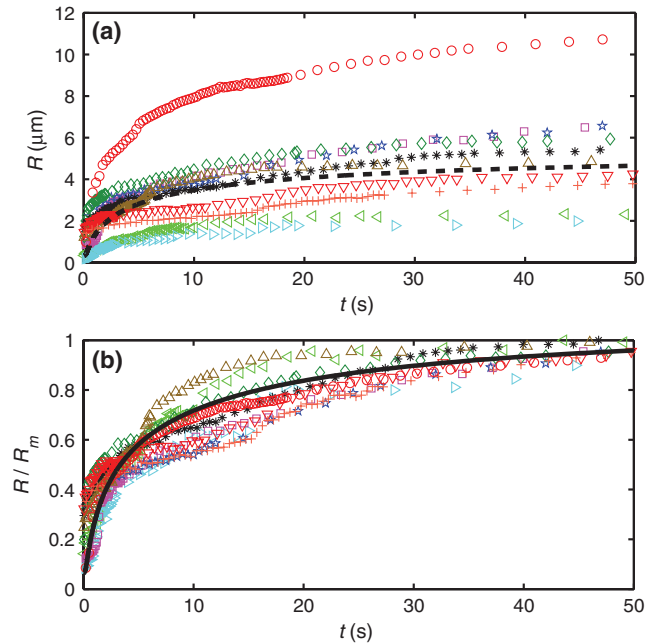
FIG. 4 (color).   (a) Evolution of the TEM radius R with time. The different symbols correspond to different experimental realizations, and the dashed line is the model's prediction for a typical set of parameter values. (b) Evolution of the TEM radius normalized by the maximum radius for each experiment, and normalized theoretical prediction (full line).

*davidgr@alum.mit.edu

[1] E. Lemichez, M. Lecuit, X. Nassif, and S. Bourdoulous, Nat. Rev. Microbiol. **8**, 93 (2010).

[2] P. Munro, M. Benchetrit, M. A. Nahori, C. Stefani, R. Clément, J. F. Michiels, L. Landraud, O. Dussurget, and E. Lemichez, Infect. Immun. **78**, 3404 (2010).

[3] M. P. Maddugoda, C. Stefani, D. Gonzalez-Rodriguez, J. Saarikangas, S. Torrino, S. Janel, F. Prodon, A. Doye, P. L. Goossens, F. Lafont, P. Bassereau, P. Lappalainen, F. Brochard-Wyart, and E. Lemichez, Cell Host Microbe **10**, 464 (2011).

[4] L. Boyer, A. Doye, M. Rolando, G. Flatau, P. Munro, P. Gounon, R. Clément, C. Pulcini, M. R. Popoff, A. Mettouchi, L. Landraud, O. Dussurget, and E. Lemichez, J. Cell Biol. **173**, 809 (2006).

[5] P. Chardin, P. Boquet, P. Madaule, M. R. Popoff, E. J. Rubin, and D. M. Gill, EMBO J. **8**, 1087 (1989).

[6] H. F. Paterson, A. J. Self, M. D. Garrett, I. Just, K. Aktories, and A. Hall, J. Cell Biol. **111**, 1001 (1990).

[7] A. B. Jaffe and A. Hall, Annu. Rev. Cell Dev. Biol. **21**, 247 (2005).

[8] Y. Cai, O. Rossier, N. C. Gauthier, N. Biais, M.-A. Fardin, X. Zhang, L. W. Miller, B. Ladoux, V. W. Cornish, and M. P. Sheetz, J. Cell Sci. **123**, 413 (2010).

[9] See Supplemental Material at http://link.aps.org/supplemental/10.1103/PhysRevLett.108.218105 for a movie showing a typical TEM opening event.

[10] P.-G. de Gennes, F. Brochard-Wyart, and D. Quére, *Capillarity and Wetting Phenomena: Drops, Bubbles, Pearls, Waves* (Springer, New York, 2004).

[11] C. Redon, F. Brochard-Wyart, and F. Rondelez, Phys. Rev. Lett. **66**, 715 (1991).

[12] C. Redon, J. B. Brzoska, and F. Brochard-Wyart, Macromolecules **27**, 468 (1994).

[13] O. Sandre, L. Moreaux, and F. Brochard-Wyart, Proc. Natl. Acad. Sci. U.S.A. **96**, 10591 (1999).

[14] W. Helfrich, Z. Naturforsch. C **28**, 693 (1973).

[15] R. Lipowsky, *Handbook of Biological Physics* (Elsevier, New York, 1995), Chap. 5.

[16] A. Mogilner and G. Oster, Biophys. J. **71**, 3030 (1996).

[17] D. Raucher and M. P. Sheetz, J. Cell Biol. **148**, 127 (2000).

[18] C. T. Walsh, D. Stupack, and J. H. Brown, Mol. Interv. **8**, 165 (2008).

[19] K. Guevorkian, M.-J. Colbert, M. Durth, S. Dufour, and F. Brochard-Wyart, Phys. Rev. Lett. **104**, 218101 (2010).

[20] S. Douezan, K. Guevorkian, R. Naouar, S. Dufour, D. Cuvelier, and F. Brochard-Wyart, Proc. Natl. Acad. Sci. U.S.A. **108**, 7315 (2011).